JOURNAL OF AIRCRAFT
Vol. 47, No. 4, July–August 2010

Experimental Characterization of Limit Cycle Oscillations in Membrane Wing Micro Air Vehicles

Jordan W. Johnston,* Will Romberg,* Peter J. Attar,† and Ramkumar Parthasarathy‡
University of Oklahoma, Norman, Oklahoma 73072

DOI: 10.2514/1.47258

The idea of using small-scale vehicles, often termed micro air vehicles, for various surveillance applications has become increasingly popular in recent years. A micro air vehicle design of particular interest is the membrane wing micro air vehicles, in which the structural skeleton is covered with a thin membrane instead of conventional wing skin materials, developed in particular for its lightweight nature, static stability, and passive gust rejection. In the current work, membrane wing micro air vehicles are developed and tested experimentally in order to determine the structural response of batten-reinforced membrane wing micro air vehicles to varying conditions: small angles of attack, number of battens, and membrane pretension. A self-excited instability (flutter) was noted for each model with limit cycle oscillations occurring at postflutter flow velocities. Small angles of attack had little effect on the flutter velocity, frequency, and mode for a given configuration, while increasing the membrane pretension delayed flutter and reduced the magnitude of limit cycle oscillation experienced by the model at a given flow velocity. Increasing the number of structural battens for the membrane wing micro air vehicle models also delayed the flutter velocity and reduced the magnitude of limit cycle oscillation at a given flow velocity while altering the flutter mode.

I. Introduction

IN RECENT years, the need for smaller, readily deployable, and easily controlled aircraft has become more pressing. Unmanned aerial vehicles have proven their effectiveness on the world stage; the RQ-4 Global Hawk and the MQ-1 Predator have provided remarkable support in Afghanistan and Iraq.[§] Recently, however, a new class of vehicle has begun to take shape: micro air vehicles (MAVs). MAVs are most commonly defined as vehicles with a major dimension less than 6 in. operating at flight speeds less than 25 mph [1]. Ideally suited to the role of reconnaissance because of their size and agility, MAVs have the ability to fulfill a wide range of applications, from military to exploratory, and have even been proposed as a first warning and monitoring system for disaster zones [2].

MAVs have also proven difficult to control, as their small size and weight prevents the use of conventional control techniques. Because of their small size, these vehicles are also very susceptible to disturbances, such as atmospheric gusts. Recently a new type of MAV has been developed, which is capable of reducing the amount of control input necessary to maintain flight [1]. These membrane wing MAVs (MMAVs) have lifting surfaces that resemble bats' wings and consist of a lightweight structural skeleton covered with a latex rubber membrane skin. Of particular importance to the MMAVs is the passive ability of the wing skin to change shape to reflect flight conditions. Termed adaptive washout by Albertani et al. [3], this effect has been shown to reduce drag, give improved stall behavior, and allow for passive gust rejection.

Several factors dictate the performance of a membrane wing MMAV in-flight, including skeletal layout, stiffness, and membrane prestrain. Ifju et al. [1] presented methods for the design and construction of a variety of flexible wing MAVs, as well as some discussion on experimental testing using visual image correlation (VIC), and demonstrated that the adaptive nature of the flexible wing design greatly improved stability and reduced drag. The effect of batten thickness and spacing on MMAVs during flight was explored by Abudaram et al. [4], where it was shown that thin (less stiff) battens led to reduced wing bending and adaptive washout, while thick battens were unable to alleviate flight loads and therefore demonstrated increased wing bending and, in some cases, wash-in. Thicker battens also demonstrated delayed stall and higher peak lift coefficients.

Rojratsirikul et al. [5] investigated experimentally the effect of membrane prestrain and excess length on the fluid-structure interaction of two-dimensional membrane wing airfoils using digital particle image velocimetry (PIV). The airfoils were tested with prestrains of $\delta = 0$, 2.5, and 5% at angles of attack varying from 9–30 deg and flow velocities of 5, 10, and 15 m/s. Membrane tension was dominated by membrane pretension for low flow velocities, gradually increasing to a uniform value for all cases of pretension; this study also indicated that models with pretension exhibited large flow-separation regions.

The effect of structural stiffness on the aerodynamic response of MMAVs was studied by Hu et al. [6]. Five MAVs were constructed using identical airfoils; the first was constructed entirely out of unidirectional carbon fiber to serve as a rigid basis, while the remaining four were constructed to be batten-reinforced (BR) MMAVs. The number of battens was varied between models (1, 2, 3, and 10). The aerodynamic performance of the various structures was analyzed in conjunction with PIV. The results showed that BR MMAVs of extremely low stiffness, such as the one-batten model, were too flexible to maintain the airfoil shape during flight and provided the lowest L/D of any of the models. The remaining BR models provided delayed stall, reduced drag, and higher L/D as compared to the rigid airfoil wing models. It was also shown that a significant increase in battens and therefore stiffness, as in the case of the 10-batten model, provided very similar aerodynamic performance to the rigid airfoil model. PIV measurements showed that at higher angles of attack (AOA > 10 deg), the rigid airfoil underwent flow separation, while the BR models deformed, reducing the effective angle of attack (AOA), and allowing flow to stay attached longer. Vibrations of the membrane skins of BR models were noted for low angles of attack (AOA < 10 deg).

The effect of the high degree of flexibility of MMAVs on aerodynamic performance has also been investigated computation-

Received 18 September 2009; revision received 9 December 2009; accepted for publication 9 December 2009. Copyright © 2009 by Jordan Johnston. Published by the American Institute of Aeronautics and Astronautics, Inc., with permission. Copies of this paper may be made for personal or internal use, on condition that the copier pay the $10.00 per-copy fee to the Copyright Clearance Center, Inc., 222 Rosewood Drive, Danvers, MA 01923; include the code 0021-8669/10 and $10.00 in correspondence with the CCC.

*Graduate Student. Member AIAA.
†Assistant Professor, School of Aerospace and Mechanical Engineering. Senior Member AIAA.
‡Professor, School of Aerospace and Mechanical Engineering. Associate Fellow AIAA.

§Data available online at http://www.af.mil/ [retrieved 16 February 2009].

ally in several studies. A comprehensive review of MAV performance characteristics and current research was provided by Shyy et al. [7], with particular emphasis on the effects of low aspect ratio and AOA on wing-tip vortices, laminar-boundary-layer separation, stall characteristics, and vibrations in MMAVs. Several combinations of computational fluid dynamics (CFD) and finite element techniques are presented in other works. Lian and Shyy [8] compared the aerodynamic performance of a rigid wing to that of a BR MMAV and showed them to have comparable prestall performance, while the MMAV demonstrated delayed stall and increased lift poststall. Similar results were found in the works of Gordnier [9] and Gordnier and Attar [10], who used a sixth-order Navier–Stokes solver coupled with a membrane structural solver in order to calculate the membrane deflections, aerodynamic performance, and resulting flow structures of a membrane airfoil. Stanford et al. [11] characterized the deflection of a membrane wing using steady-state CFD and finite element modeling. The computed MMAV pressure distributions and static structural deflections were compared to experimental VIC results. Results of this study identified Hooke's law as an accurate means of approximating the prestress of the stretched membrane, despite latex rubber's hyperelastic material properties.

While it seems clear that the aerodynamic performance at low Reynolds number can be enhanced by the intentional introduction of added flexibility to the wing, doing so will likely cause MMAVs to be more susceptible to unwanted aeroelastic phenomena, such as static divergence, flutter, limit cycle oscillation (LCO), and buffet. Therefore, the aim of the current paper is to study the aeroelastic response of a BR MMAV to varying membrane prestrains, flow velocities, and small angles of attack. In particular, the effects of these parameters on the flutter and LCO behavior of BR MMAVs at low angles of attack will be characterized through experimentation. Structural frequency and peak displacement response results for several different membrane prestrain configurations (2, 5, 7, and 10% at 0, 1, and 2 deg angles of attack) will be presented along with experimental results, which compare the flutter and limit cycle behavior of BR MMAVs with differing batten materials (aluminum and composite) and batten configuration.

II. Experimental Techniques

A. Wind Tunnel

Experimental testing is conducted within the University of Oklahoma's low-speed wind tunnel: an open-loop, closed-throat wind tunnel with a circular test-section inner diameter of 45.7 cm and length of 76.2 cm and constructed of clear Plexiglas. The wind tunnel is capable of producing flow velocities of 1.5 to 34 m/s and is driven by an ILG ducted fan and a 40 hp GE induction motor. The flow velocity is controlled by varying the rotational frequency of the motor using an Eaton SVX9000 electric motor controller. For the purpose of the current work, only flow velocities of 1.5 to 8.5 m/s are used.

B. Membrane Wing Models

The BR half-span membrane wing used for this experiment is shown in Fig. 1. It is a flat-plate rectangular wing with a span of 15.2 cm and an aspect ratio of 0.75 for a full-span model. The model is mounted vertically in the wind tunnel, as shown in Fig. 1.

Wing battens measure 0.64 cm wide and a 5.10 cm foot is built into the bottom of the wing at a 90 deg angle to facilitate mounting. Each model consists of a two-, three-, four-, or five-batten skeletal framework covered in 0.15-mm-thick latex. Two materials are used for the construction of the skeleton: carbon fiber and aluminum. For the case of the carbon fiber model, the wing is molded in a wet layup/vacuum bag, built up using four layers of 4 harness satin carbon fiber weave for the outer battens and leading edge and two layers for the middle batten. A U.S. Composites two-part epoxy is used for the matrix: 635 thin epoxy resin and a 3:1 of epoxy hardener. This results in an approximate thickness of 0.79 mm. Aluminum models are machined out of 1.59-mm-thick 6013 T4 aluminum.

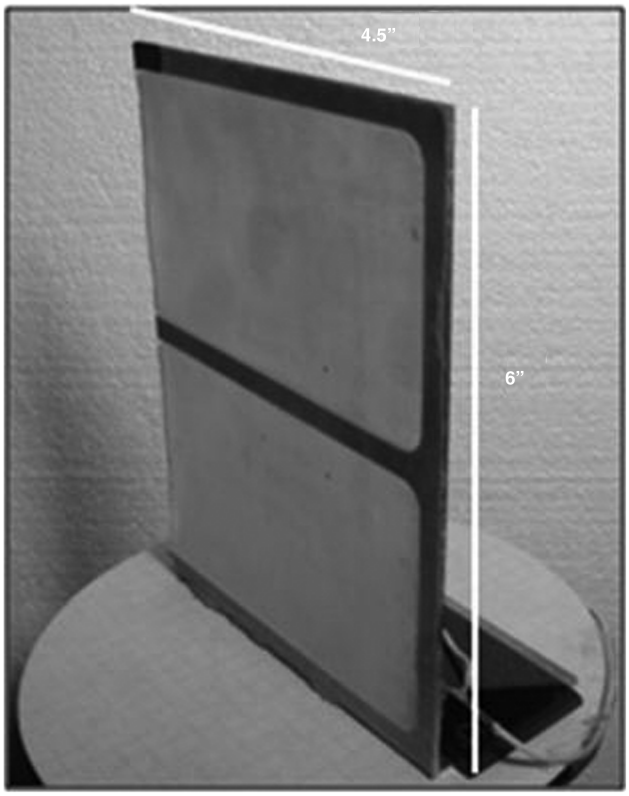

Fig. 1 A mounted three-batten MMAV with a prestrain of 5%.

The circular frame shown in Fig. 2a is used to uniformly stretch latex to the desired prestrain before application to the skeleton. The frame consists of two pieces held together at the corners by machine screws. Unstrained latex is clamped between the two halves and stretched over a pedestal, as shown in Fig. 2b, the height of which determines the strain placed on the latex. Prestrain for a given height is determined by measuring the distance between markings placed on the unstrained latex at a known distance. 3M General Trim Adhesive is then applied to the skeleton, which is then firmly pressed into the pedestal. After curing, the excess latex is trimmed away. For the current work, prestrains in both the chordwise and spanwise directions of 2, 5, 7, and 10% are considered. Prestrain is determined by marking the unstretched latex at three points, 2.54 cm apart. After stretching, the distance between the marks is determined with a pair of dial calipers. The estimated accuracy of the prestrain on any MMAV model is $\pm 0.2\%$.

C. Imaging

Membrane and batten deformation data are collected through the use of a MotionPro X3 high-speed camera using a 25 mm Fujinon lens connected to a dedicated Sony Vaio laptop. Resolution is set so that a single pixel measures 0.0178 cm wide; this is to ensure that the focus remains constant and repeatable between tests. The camera is mounted directly above the model on the outer wall of the test section and records at 1250 frames/second for a total of 2.5 s. Two 250 W halogen lamps provide lighting of the model. Image analysis is carried out using the software MotionPro Studio; deformations are calculated based on image pixel width and a reference scale built into the specimen's mounting fixture. Recordings are taken at flow velocities ranging from 1.5 to 8.5 m/s in increments of 0.5 m/s. For each video produced, 10 measurements of membrane wing skin deflection are recorded. Five measurements correspond to the positive deflection experienced by the membrane wing skin, and five measurements correspond to negative deflection. Each of these data points represents a maximum deflection, either in the positive or negative direction, spread evenly in time across the 2.5 s of the high-speed footage. Positive and negative deflection values are recorded in pairs, corresponding to one period of oscillation. Data recorded from

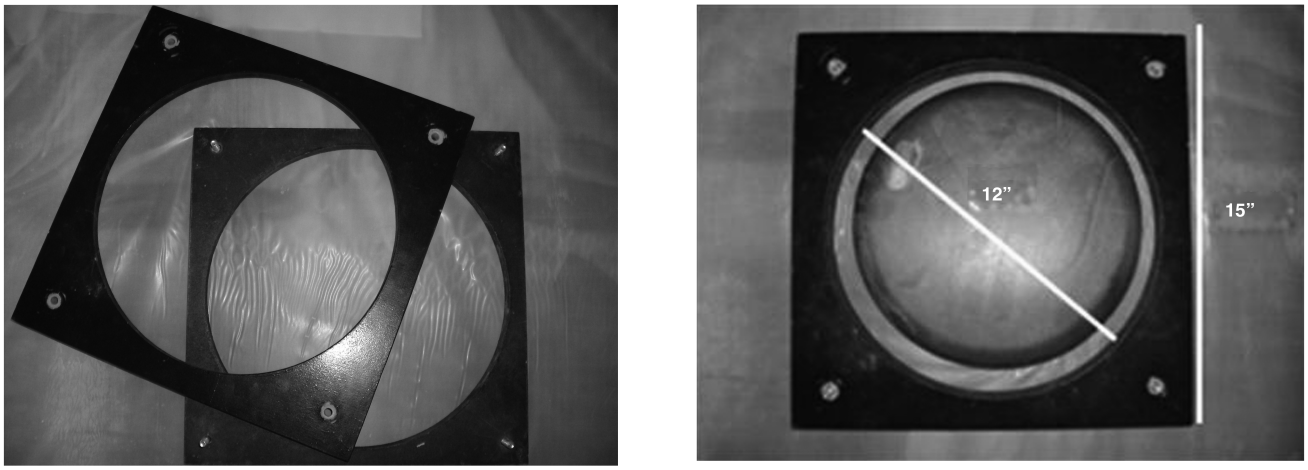

a) b)

Fig. 2 Latex stretching frame.

each video for positive and negative deflections are then averaged and subsequently reported. Uncertainty in the current work is primarily caused by image quality, which results in a least count of 0.0178 cm for any given reading. To quantify the level of uncertainty, six recordings were taken of a given batten/prestrain/AOA configuration (four battens, 5% prestrain, 0 deg AOA) at a single flow velocity in the postflutter regime. Ten latex deflection measurements were recorded for each video recording, as described above. The uncertainty analysis was performed, as described in [12], using 30 data points each for positive and negative deflection, and the maximum uncertainty in the measurement of the deflection of the latex membrane wing skin was found to be ± 0.032 cm with 95% confidence.

D. Strain Data

Strain gauges are used to determine the model's dynamic response characteristics as well as provide point strain data. Each model is equipped with a strain gauge located at 3.10 cm from the root and 0.32 cm from the leading edge. A Vishay model WK-06-031CF-350 strain gauge is used and is applied using M-Bond 200. Strain data are recorded on a dedicated Dell laptop through a National Instruments (NI) cDAQ-9172 chassis using a four-channel NI 9237 module and an NI 9945 bridge completion module. Data are sampled at 1250 Hz for 2.5 s and stored in an Excel spreadsheet. Testing has shown that LCO of the membrane skin generally occurs at a frequency on the order of 100 Hz, allowing the strain data recorder to capture more than 200 complete cycles.

E. Testing Methodology

As mentioned previously, testing is performed with a wide range of membrane prestrains and three angles of attack. Each MMAV model, with a two-, three-, four-, or five-batten skeletal layout, is constructed with a desired prestrain, 2, 5, 7, or 10% and tested for angles of attack of 0, 1, and 2 deg for the velocity range of 1.5 to 8.5 m/s: a Reynolds number range of 11,000 to 64,000. In the tests, the tunnel velocity was increased from zero by increasing the rotational frequency of the wind-tunnel motor through an electronic motor controller. The smallest increments in motor frequency possible were 0.5 Hz, which corresponds with a change in flow velocity of approximately 0.5 m/s. Once a motor speed was set, the flow was allowed to reach a steady velocity and then measurements were started. Once measurements were completed at a given flow velocity, the motor rotational frequency was increased to a higher value for the next measurement. High-speed-camera and strain-gauge data are recorded throughout each test, which is then repeated a second time to provide a measure of the repeatability of the experiment.

III. Results

A. Flutter

All discussion in this section refers to models constructed with three battens. As stated in Sec. II.D, the smallest possible increment in the wind-tunnel flow of velocity is 0.5 m/s; hence, figures that present flutter velocity results should be interpreted accordingly (e.g., the results presented are accurate to within ± 0.25 m/s).

Figure 3 shows the variation of flutter onset speed with prestrain for the cases of three-batten aluminum MMAVs for all three angles of attack, as well as that of a three-batten carbon fiber MMAV at 1 deg AOA.

As the plot demonstrates, the flutter velocity more than doubles over the range of prestrain values that were tested (2–10%). As shown in Fig. 3, it is also apparent that the flutter velocity is relatively independent of AOA for the range of angles tested. It is interesting to note that the 5% prestrain carbon fiber model, with a frame of significantly reduced thickness and weight as compared to the aluminum configurations, has a flutter velocity that is very similar to the corresponding aluminum configuration. This is likely due to the mode of flutter, which is primarily localized to the membrane portions of the configuration in each case, causing the membrane prestrain to be the dominant factor influencing the flutter speed.

Figure 4 shows images taken of the airfoil during postflutter LCO (to be discussed in the next section) at four time steps evenly spaced throughout one period of oscillation for a flow velocity of 5.2 m/s, a latex prestrain of 5%, and an AOA of 0 deg. The leading edge of the airfoil is not in view of the camera, but is located at the top of each image. What can be seen is 1.5 in. of the trailing edge mounted to the wind tunnel. As previously mentioned, there is a 5.08 cm foot built

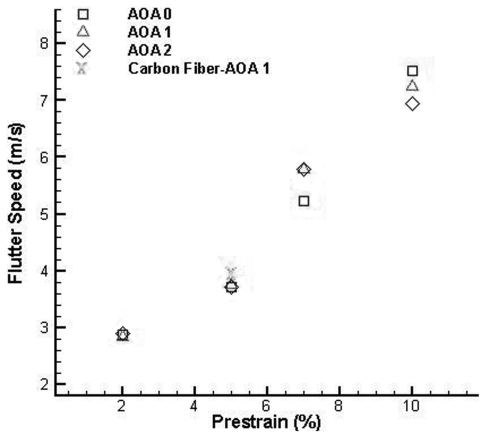

Fig. 3 Flutter velocity as a function of the level of latex prestrain.

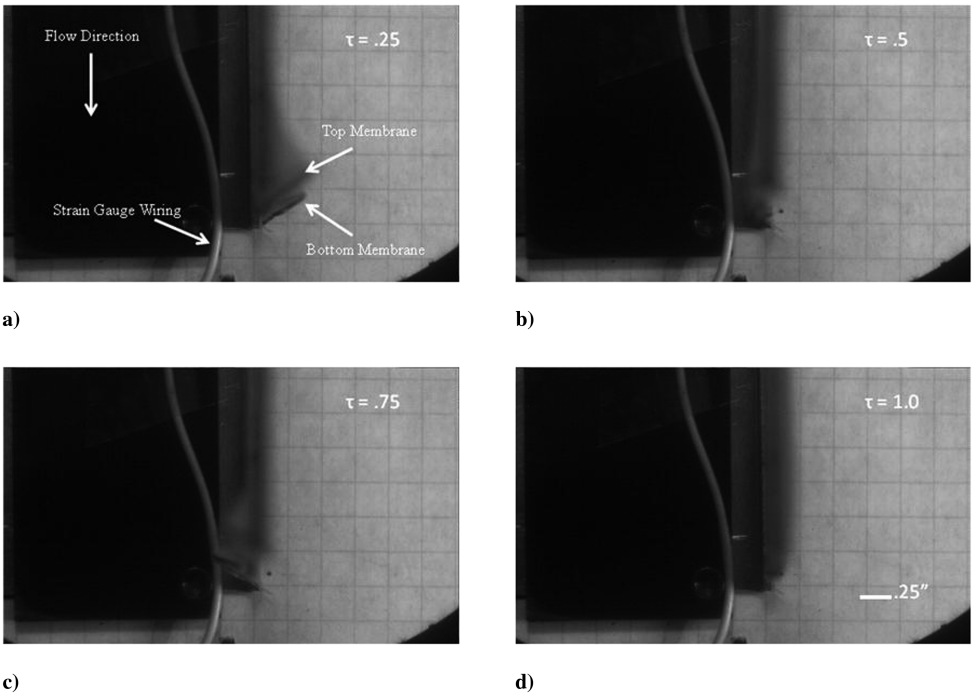

Fig. 4 Representative flutter mode over one period of oscillation.

into the model for mounting purposes, and the mount can be seen to the left as a black plate, separated 0.64 cm from the model to prevent any interference. The airfoil is mounted with a 0.64 cm grid at the base to facilitate deflection measurements. Image resolution provides a clear and accurate picture of both positive and negative membrane wing skin deflections, resulting in a uniform uncertainty in deflection measurements. At the first time $\tau = 0.25$, both the top and bottom membrane panels are in phase and have reached their peak positive deflection. Here (and elsewhere in the text), the terms top and bottom panels refer to the membrane panels that are closest to the wing tip and wing root, respectively. At time $\tau = 0.5$, the panels are moving toward the underside of the wing and are seen just crossing the midplane of the airfoil. The peak negative deflection can be seen at $\tau = 0.75$, where, again, the top and bottom membrane panels are in phase. The final time $\tau = 1.0$ shows the panels once again crossing the midplane of the airfoil and moving toward the upper surface of the airfoil. While this particular flutter mode is not present in all of the models tested, it is the mode most often seen in the experiments. Variations in this mode of response include out-of-phase membrane panel oscillation, a modulated response, and a trailing-edge flip of the membrane panel. Each of these variations will be demonstrated and discussed later in this work.

The flutter frequency vs prestrain for all angles of attack, determined from a discrete Fourier transform (DFT) of the strain-gauge readings, is shown in Fig. 5. Only the dominant (highest magnitude Fourier coefficient) frequency is extracted from the DFT and plotted.

Similar to the flutter velocity results shown in Fig. 3, the flutter frequency is not a strong function of AOA at a given value of membrane prestrain. Also, it should be noted that for the highest prestrain level of 10%, multiple dominant frequencies are noted in the DFT results. This is shown in Figs. 6a and 6b, which are DFTs of the signal at two flow velocities for the 10% model at 0 deg AOA.

B. LCO Response with Changing Prestrain and AOA

In each of the cases tested, LCOs are noted for postflutter flow velocities. Figures 7–9 show the magnitude of LCO, defined here as the maximum deformation of the midpoint of the bottom membrane panel vs flow velocity for a set AOA and various prestrain levels. Shown in these figures are both the maximum positive and negative membrane oscillations recorded from two complete runs of the velocity spectrum (1.5 to 8.5 m/s).

From these figures, it is clear that the 2% prestrain case exhibits the highest magnitude across the velocity range, regardless of AOA, exceeding a displacement of 1 cm at the higher flow velocities and shows a steady increase throughout the velocity range. On the other hand, for each AOA, the 5% case demonstrates two different behaviors depending on flow velocity. Between the range of 3.75 to 5.20 m/s, there is a band of near-constant displacement, after which the displacement grows steadily to a value near 1 cm. Later plots will further demonstrate this behavior.

It is interesting to note that at approximately the same flow velocity; as the displacement increase described in the preceding paragraph is observed in models with 5% prestrain, those models with 7% prestrain become unstable and undergo a limit cycle with nearly the same magnitude, as is observed in the 5% prestrain models. After flutter begins, the magnitude remains close to, but always less than, that of the 5% prestrain. Overall, it appears that at a given postflutter flow velocity and AOA, the LCO response decreases with increasing prestrain. Demonstrating the lowest magnitude of displacement for the velocity range tested, models with 10% prestrain exhibit the most dramatic increase in displacement from the onset of flutter to the end of the test spectrum, ending at a magnitude of approximately 0.625 cm for the highest velocity tested.

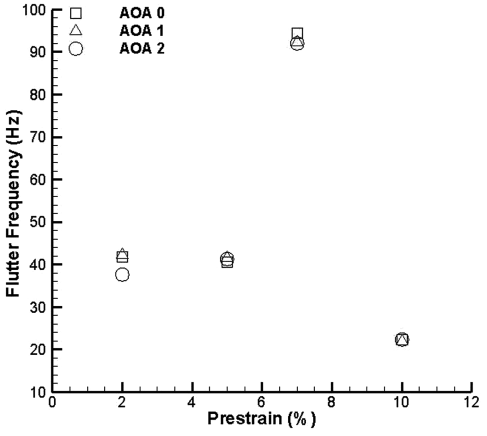

Fig. 5 Flutter frequency as a function of the level of latex prestrain.

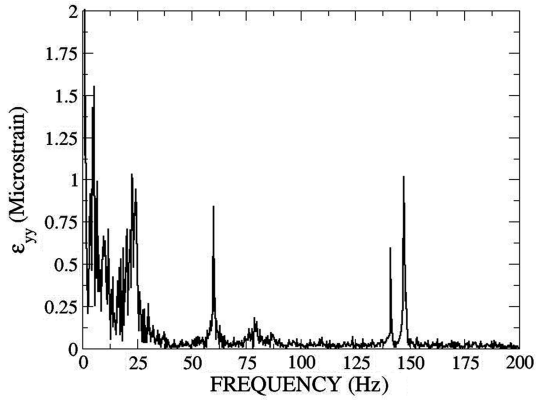

a)

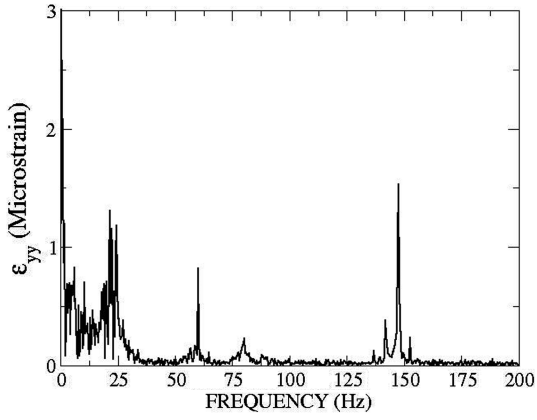

b)

Fig. 6 DFT plots for strain response for a) 10% prestrain at 0 deg AOA and 7.53 m/s flow velocity and b) 10% prestrain at 0 deg AOA and 8.40 m/s flow velocity.

To show the variation of LCO response with small angles of attack, Figs. 10–13 show the positive and negative LCO magnitude for a given value of prestrain vs flow velocity for all angles of attack tested.

Figure 10 reveals that for the 2% prestrain case at a given flow velocity, the magnitude of LCOs are very similar between angles of attack, a trend that is generally repeated in all of the prestrain cases. A slight increase in LCO magnitude (both positive and negative) with AOA is noted for the 2 and 5% prestrain cases, while a slight decrease in magnitude with increasing AOA is measured for the 7 and 10% cases. However, the differences are not dramatic.

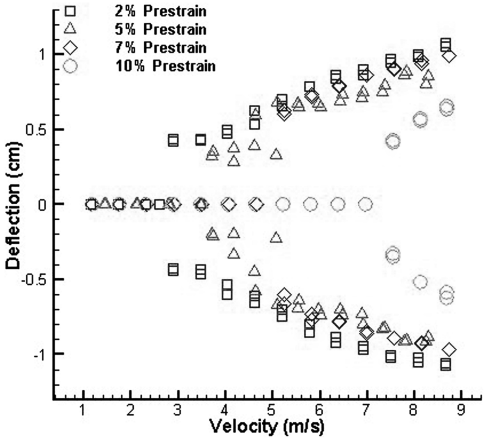

Fig. 7 LCO magnitude vs flow velocity for all levels of prestrain at an AOA of 0 deg.

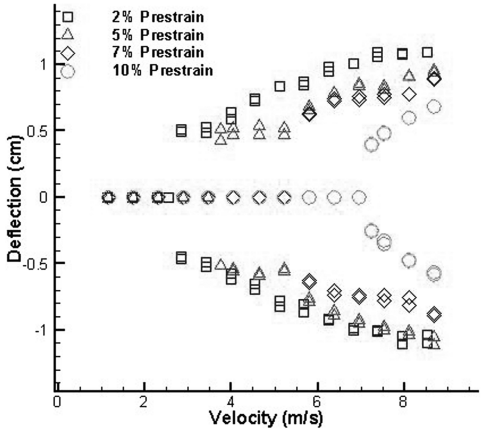

Fig. 8 Magnitude vs flow velocity for all levels of prestrain at an AOA of 1 deg.

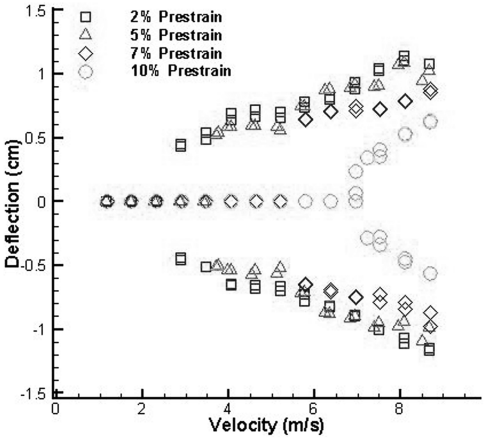

Fig. 9 Magnitude vs flow velocity for all levels of prestrain at an AOA of 2 deg.

In Fig. 11, the LCO magnitude results for the 5% prestrain case are shown. Qualitatively, the dependence on the LCO magnitude with flow velocity is similar for each AOA with three tiers of displacement occurring across the velocity range. It is interesting to note that, in this case (5% prestrain), the negative LCO is higher in magnitude than the positive LCO for all angles of attack.

Figure 12 is a plot of the LCO magnitude vs flow velocity for the 7% prestrain case. Unlike the 2 and 5% prestrain cases, the 7% case exhibits the highest magnitude of LCO at 0 deg AOA. Also, while the

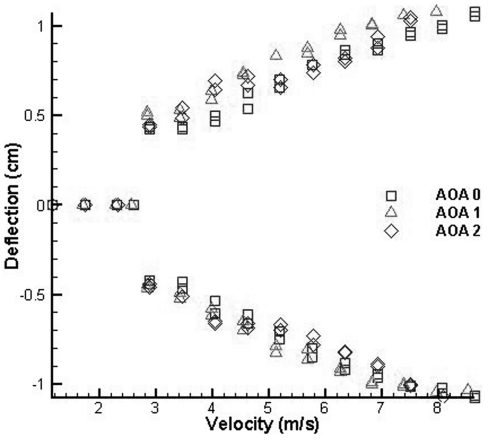

Fig. 10 LCO magnitude vs flow velocity for 2% prestrain at all angles of attack.

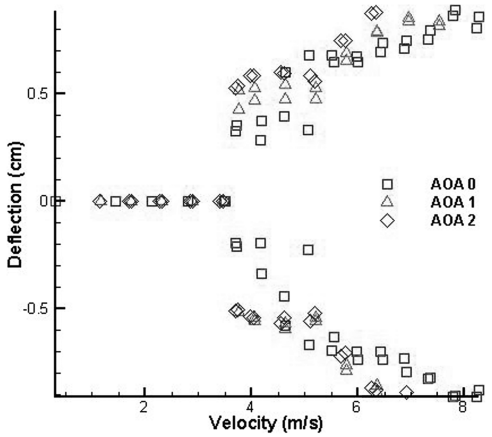

Fig. 11 LCO magnitude vs flow velocity for 5% prestrain at all angles of attack.

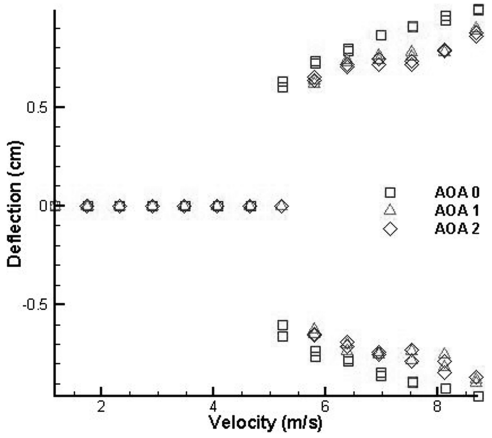

Fig. 12 LCO magnitude vs flow velocity for 7% prestrain at all angles of attack.

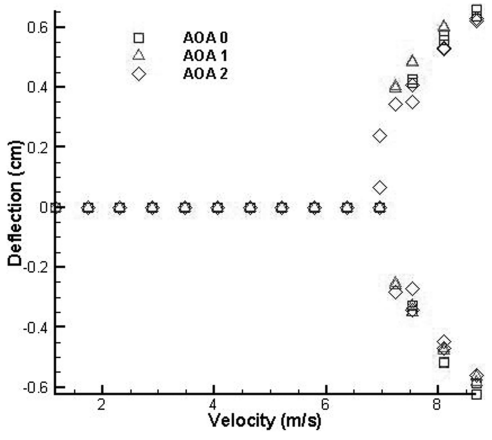

Fig. 13 LCO magnitude vs flow velocity for 10% prestrain at all angles of attack.

magnitude of LCOs are similar, there does appear to be a clear qualitative difference in the 0 deg AOA and non-0-deg AOA LCO curves. At 0 deg AOA, the magnitude of LCO steadily increases with flow velocity, while at non-0-deg AOA, a region of flow velocity (between 7 and 8 m/s) is observed where the LCO magnitude does not increase resulting in a plateau in the LCO curve. This flattening of the LCO curve was also noted for the 5% prestrain case for each of the angles of attack.

In the case of the 10% prestrain configurations, the LCO magnitudes (as shown in Fig. 13 vs flow velocity) are once again similar across the range of angles of attack tested (within 0.05 cm for a given flow velocity). However, unlike the other prestrain cases, at a fixed flow velocity, the 10% case shows a significant difference of approximately 16% in the positive and negative values of LCO magnitude.

Figure 14 is a plot of the LCO magnitude vs normalized (by the configuration flutter velocity) flow velocity for each of the four membrane prestrain cases at an AOA of 0 deg. From this figure, it appears that an increase in membrane prestrain not only results in an increase in flutter speed, as has been noted in the previous figures, but also in an increase in LCO magnitude at a certain percentage of the flow velocity above the flutter speed. It is clear from Fig. 14 that this is certainly true when going from 7% prestrain to 5% prestrain and, to a lesser extent, when going from 5 to 2%. It is unclear whether the trend also holds when going from 10 to 7%, as there are not enough data points to clearly discern the effect.

Overall, it appears that the nonlinear mechanism(s) that are limiting the response postflutter are strong, which is clearly demonstrated by the slow increase in LCO magnitude with flow velocity. This is most evident in the 2, 5, and 7% prestrain cases. It is also clear that this mechanism is a weak function of the static AOA for the range of these angles tested, as generally very little change in the qualitative and quantitative nature of the LCO curves is noted with change in AOA for a given prestrain value.

An inspection of the LCO frequencies reveals some more trends of interest. Figures 15–18 show the DFT frequency results as a function of velocity for individual prestrains at an AOA of 0 deg. These frequencies are chosen by taking a DFT of the strain response and choosing the frequency that corresponds to the largest magnitude Fourier coefficient.

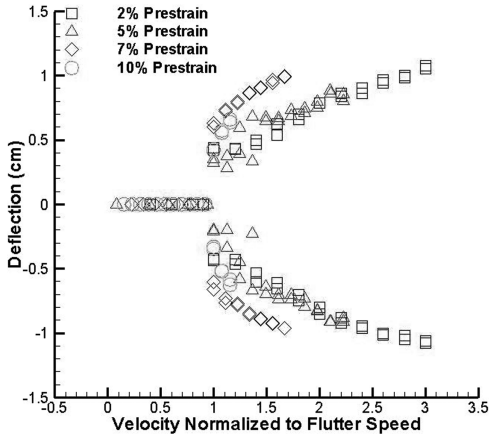

Fig. 14 LCO magnitude vs normalized (by respective flutter velocity) flow velocity for all prestrain, three-batten configurations at 0 deg AOA.

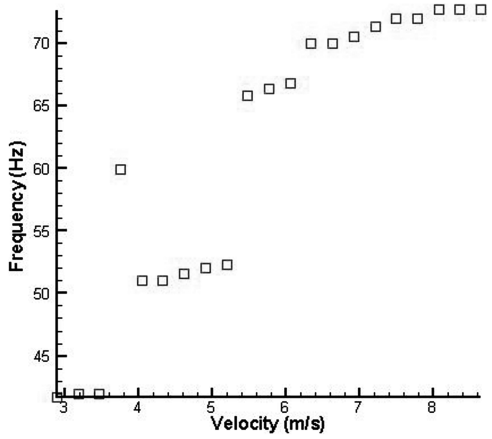

Fig. 15 LCO frequency vs flow velocity for 2% prestrain at an AOA of 0 deg.

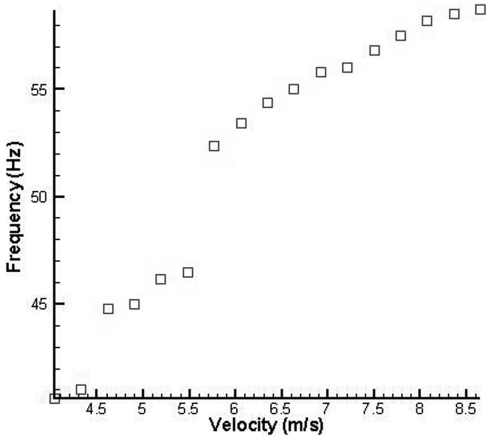

Fig. 16 LCO frequency vs flow velocity for 5% prestrain at an AOA of 0 deg.

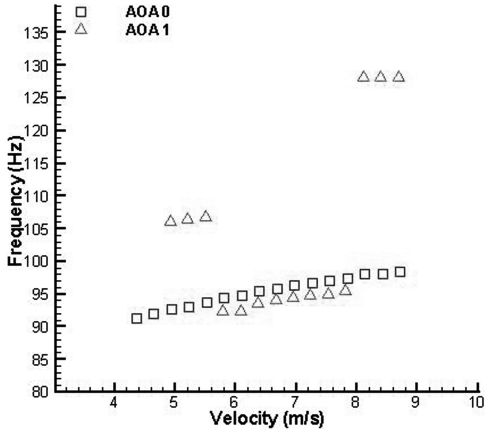

Fig. 17 LCO frequency vs flow velocity for 7% prestrain at angles of attack of 0 and 1 deg.

In Fig. 15, it can be seen that the 2% prestrain model exhibits three different levels at which the frequency remains almost constant; similar behavior is seen in the 5% prestrain model at the lower flow velocities (see Fig. 16). As shown in Fig. 17, at an AOA of 0 deg, the LCO response for the 7% prestrain case varies smoothly across the range of flow velocities from a value of approximately 95 Hz just before flutter begins to a value of approximately 97 Hz at the highest flow velocity.

In Fig. 18, the 10% prestrain model LCO frequency is plotted vs flow velocity. Unlike the other prestrain levels, where at a given flow velocity one frequency is dominant in the DFT results, the 10% case exhibits two frequencies, approximately 25 and 140 Hz, with very similar magnitude Fourier coefficients that trade dominance when the flow velocity is varied. This can be clearly seen in DFT results shown in Figs. 6a and 6b, which show the two primary competing frequencies.

For the 2, 5, and 10% cases, the LCO frequency content at a given flow velocity is very similar for 0 and non-0-deg AOA. The 7% prestrain model displays slightly different behavior at a non-0-deg AOA. For this prestrain level at non-0-deg AOA, in the flow velocity region near (but before) to the flutter velocity, a higher frequency of 106 Hz is dominant. After the onset of flutter, the dominant frequency decreases to 95 Hz, as seen previously in the 0 deg AOA case. A final change occurs at about 8 m/s when the frequency climbs to a value near 128 Hz.

C. LCO Response with Varying Batten Configurations

To determine the effect of the number of battens on the LCO characteristics, four models with an identical prestrain of 5% are constructed with two, three, four, and five battens. All four models are tested at the same AOA of 0 deg across the same velocity spectrum: 1.5 to 8.5 m/s. Figure 19 shows the LCO response for these MAVs.

These results indicate two important features of increasing structural stiffness through the addition of battens. First, there is a significant increase in flutter velocity with increasing number of battens, ranging from approximately 2.25 m/s with two battens to approximately 8.35 m/s with five battens. Second, there is a drastic reduction in LCO magnitude at a given flow velocity with increasing number of battens, as well as a flattening of the LCO curves. In the case of the two-batten model, there is a slight plateau of magnitude of 1 cm immediately following LCO onset. Starting at approximately 2.9 m/s, the LCO magnitude begins to grow to a maximum deflection of 2.7 cm at approximately 7.5 m/s before leveling off. Increasing the number of battens to three causes a reduction in the maximum LCO magnitude of nearly 70% (from a value of 2.69 cm to a value of 0.86 cm) at a flow velocity of 7.75 m/s. In addition, the three-batten model has a level of LCO magnitude that remains nearly constant after a flow velocity of approximately 5 m/s. Between the three- and four-batten models, there is again a reduction in LCO magnitude, though much less severe, accompanied by the same type of flat LCO curve. Though the five-batten model does not begin oscillations until late within the flow velocity test region, the results hint that it might exhibit a very similar behavior. Both points taken after LCO exhibit a nearly identical magnitude of 0.15 cm.

It was also found that increasing the number of battens causes the LCO magnitude to not only decrease at a given flow velocity but also at a given percentage of the flow velocity over the flutter speed. This is shown in Fig. 20, which is a plot of the LCO magnitude vs normalized (by the respective flutter velocity) flow velocity for each

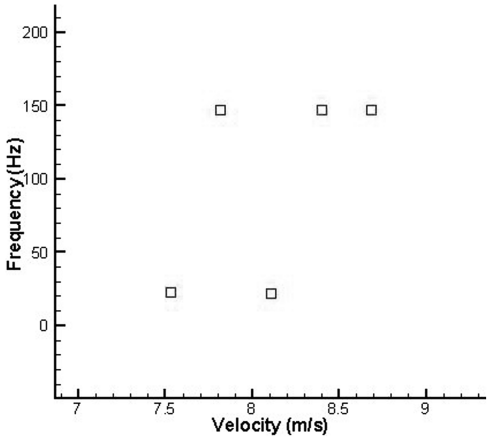

Fig. 18 LCO frequency vs flow velocity for 10% prestrain at an AOA of 0 deg.

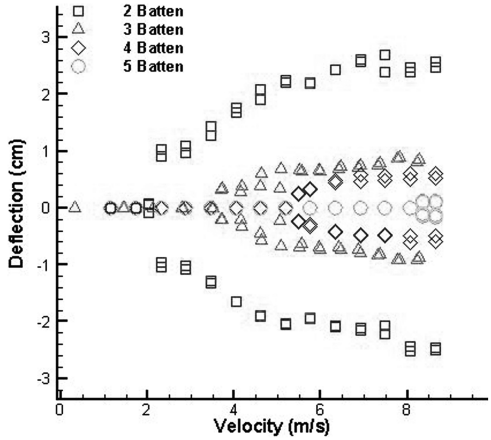

Fig. 19 LCO magnitude vs flow velocity of MMAVs of various skeletal configurations with a prestrain of 5%.

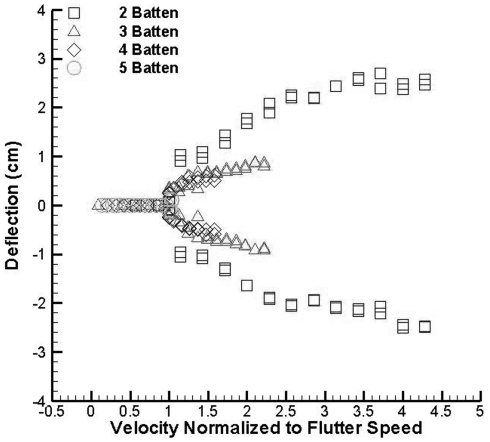

Fig. 20 LCO magnitude vs normalized (by flutter velocity) flow velocity for each batten configuration for 5% membrane prestrain and 0 deg AOA.

batten configuration at 5% prestrain and 0 deg AOA. This effect is certainly obvious when one increases from two to three battens. A further increase from three to four battens has a smaller effect, but there is still some reduction in the LCO magnitude. The result in going from four to five battens is difficult to interpret, as only a few data points postflutter were recorded for the five-batten case.

A conclusion can be from drawn from the results shown in Fig. 20 and the corresponding results shown in Fig. 14. These figures show that an increase in the frame stiffness through two separate means, the addition of battens or the addition of membrane prestrain, has an opposite effect on the LCO magnitude at a given percentage of the flow velocity above that of the configuration flutter velocity.

It is important to note that the mode of LCO is very different between the batten configurations. With only two battens, the shape of the LCO exhibits a type of trailing-edge flip, which can be seen in Fig. 21.

In Fig. 21, we can clearly see the outline of the trailing edge, picked out in black dots, as the membrane deforms. A depression forms in the membrane skin as the midpoint of the membrane panel doubles back toward the leading edge; the membrane skin is picked out in white dots to show the deformation. While similar behavior is seen in the three-batten case, it is not as severe, and is nonexistent in the four- or five-batten cases.

In the three-, four-, and five-batten cases, the modes of oscillation vary throughout each test. The shape of oscillation is very similar to that seen in Fig. 5, but with additional membrane panels, the complexity of the deformation increases. With two membrane panels, the three-batten case demonstrates both in-phase and out-of-phase oscillation of the panels, which is dependent on the flow velocity. While this does not appear to affect the overall maximum deflection of each panel or the frequencies that the structure exhibits, the local

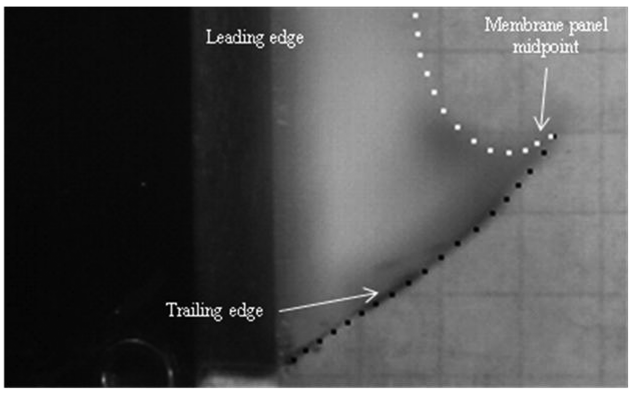

Fig. 21 Trailing-edge flip as seen with a two-batten MMAV at 0 deg AOA at a flow velocity of 8 m/s.

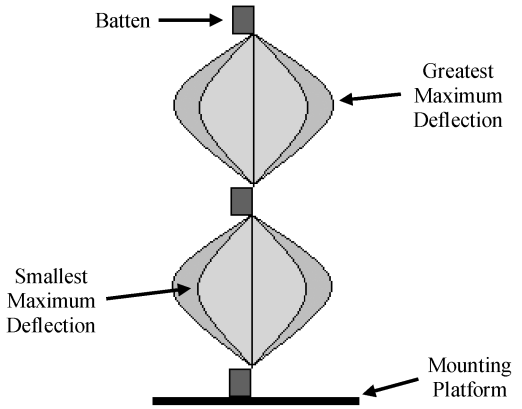

Fig. 22 Schematic of beating phenomenon as seen for the three-batten MMAV.

root-mean-square strain taken at the leading edge near the root (not presented in this work) is highly dependent on this behavior. Additional analysis, including computational modeling, of the three-batten case can be found in [13]. During the four-batten-model tests, constructed with three membrane panels, the membrane panels near the root and the wing tip remained in phase throughout the test, while the middle panel was out of phase with the other two. This behavior was repeated in tests with the five-batten model as the first (root) membrane panel was in phase with the third; the second and fourth remained in phase with each other but out of phase with the other two.

As previously mentioned, there is one other deflection shape phenomenon that occurs during LCO in these BR MMAVs: time-dependent variation of the maximum deflection (beating). This beating was not present in the two-batten case but was seen in the remaining cases. During periods of beating, each membrane panel would oscillate with a varying maximum deflection. This could be clearly seen with the naked eye as the membrane panel formed two distinct after images for each peak deflection and is sketched in Fig. 22.

While this is easily tracked during high-speed video footage, only the largest deflection was recorded for the purposes of this work. It is also worth noting that the percent difference in the magnitude of the two peaks was on average less than 10%.

IV. Conclusions

The aeroelastic behavior of BR MMAVs constructed with aluminum skeletons and latex membrane wing skins was investigated in this study. Four skeletal configurations were tested with varying latex prestrains at three different angles of attack. Experiments were conducted at flow velocities ranging from 1.5 to 8.5 m/s. Each model exhibited LCOs at different velocities within the testing range.

The experimental results reveal several trends related to the flutter/LCOs and batten configuration, prestrain, and AOA. For the three-batten configuration flutter onset appears to be primarily dependent on the physical properties of the latex and not the structural material. This is clearly seen when the flutter velocity results are compared for models with composite and aluminum frames, as very little variation in flutter velocity is seen between the two configurations. It should be noted, however, that composite frames were not used for the other batten configurations tested; hence, it is not possible to draw a general conclusion about the dependence of frame material on flutter and LCO. It is also apparent that the flutter velocity and frequency are relatively independent of AOA at small angles of attack (0, 1, and 2 deg) and that increasing the amount of latex prestrain causes a delay in the onset of flutter.

Postflutter LCOs are observed for all cases tested. It is found that the LCO magnitude decreases as the amount of prestrain is increased and is relatively independent of the (small) angles of attack that were tested. Video of the LCOs show that mode of response varies with batten configuration and includes in-phase and out-of-phase

response of the membrane panels, time dependence of the maximum deflection value (beating), and trailing-edge flip of the membrane panels. It is also noted that an increase in frame stiffness through two separate means, the addition of membrane prestrain or the addition of wing battens, has an opposite effect on the LCO magnitude at a given percentage of the flow velocity above that of the configuration flutter velocity. While increasing the membrane prestrain results in an increase in the LCO magnitude at a given normalized (by the configuration flutter velocity) flow velocity, the trend is reversed when battens are added to the wings.

Finally, spectral analyses of the LCOs show that for many of the configurations multiple dominant frequencies are present in the response. The authors find this interesting and unlike the usual limit cycle response dynamics, where one dominant frequency is normally present. Although the authors do not have a definitive answer as to why this occurs, the presence of multiple frequencies could be due to the membranes responding at their wet natural frequencies to unsteadiness in the flow because of freestream turbulence in the tunnel. In other words, the structural response could be a combined forced response due to both the unsteadiness in the freestream due to turbulence and the self-excited instability due to flutter.

The results of this study identify the flutter speeds for a variety of configurations of BR MMAVs along with trends in LCO magnitude postflutter. This information can be included in MMAV design processes, where mission-specific tailoring is necessary to reduce flight instabilities, reduce drag, and increase operational lifespan.

Acknowledgments

The authors would like to acknowledge financial support for the project provided by the University of Oklahoma Research Council and the Ohio Aerospace Institute.

References

[1] Ifju, P., Jenkins, D., Ettinger, S., Lian, Y., Shyy, W., and Waszak, M., "Flexible-Wing-Based Micro Air Vehicles," AIAA Paper 2002-705, Jan. 2002.

[2] Mohseni, K., Lawrence, D., Gyllhem, D., and Culbreth, M., "Flow Simulation Around a Micro Air Vehicle in a Plume Characterization Scenario," AIAA Paper 2004-6598, Sept. 2004.

[3] Albertani, R., Stanford, B., Hubner, P., and Ifju, P. G., "Aerodynamic Coefficients and Deformation Measurements on Flexible Micro Air Vehicle Wings," *Experimental Mechanics*, Vol. 47, No. 5, Oct. 2007, pp. 625–635. doi:10.1007/s11340-006-9025-5

[4] Abudaram, Y., Stanford, B., and Ifju, P., "Wind Tunnel Testing of Load-Alleviating Membrane Wings at Low Reynolds Numbers," AIAA Paper 2009-1468, Jan. 2009.

[5] Rojratsirikul, P., Wang, Z., and Gursul, I., "Effect of Pre-Strain and Excess Length on Unsteady Fluid-Structure Interactions of Membrane Airfoils," AIAA Paper 2009-578, Jan. 2009.

[6] Hu, H., Tamai, M., and Murphy, J., "Flexible-Membrane Airfoils at Low Reynolds Numbers," *Journal of Aircraft*, Vol. 45, No. 5, 2008, pp. 1767–1778. doi:10.2514/1.36438

[7] Shyy, W., Ifju, P., and Viieru, D., "Membrane Wing-Based Micro Air Vehicles," *Applied Mechanics Reviews*, Vol. 58, No. 4, July 2005, pp. 283–301. doi:10.1115/1.1946067

[8] Lian, Y., and Shyy, W., "Numerical Simulations of Membrane Wing Aerodynamics for Micro Air Vehicle Applications," *Journal of Aircraft*, Vol. 42, No. 4, 2005, pp. 865–873. doi:10.2514/1.5909

[9] Gordnier, R. E., "High Fidelity Computational Simulation of a Membrane Wing Airfoil," AIAA Paper 2008-614, Jan. 2008.

[10] Gordnier, R. E., and Attar, P. J., "Implicit LES Simulations of a Low Reynolds Number Flexible Membrane Wing Airfoil," AIAA Paper 2009-579, Jan. 2009.

[11] Stanford, B., Sytsma, M., Albertani, R., Viieru, D., Shyy, W., and Ifju, P., "Static Aeroelastic Model Validation of Membrane Micro Air Vehicle Wings," *AIAA Journal*, Vol. 45, No. 12, 2007, pp. 2828–2837. doi:10.2514/1.30003

[12] Mann, P., *Introductory Statistics*, 5th ed., Wiley, New York, 2004, pp. 353–371.

[13] Attar, P. J., Gordnier, R. E., Johnston, J., Romberg, W., and Parthasarathy, R., "Aeroelastic Analysis of Membrane Micro Air Vehicles," American Society of Mechanical Engineers Paper 2009-78575, Aug. 2009.